

## Physics Of Eclipsing Binaries. IX. Spectroscopic module

MIROSLAV BROŽ,<sup>1</sup> ANDREJ PRŠA,<sup>2</sup> KYLE E. CONROY,<sup>2</sup> AND MICHAEL ABDUL-MASIH<sup>3</sup>

<sup>1</sup>*Charles University, Faculty of Mathematics and Physics, Institute of Astronomy, V Holešovičkách 2, CZ-18200 Praha 8*

<sup>2</sup>*Villanova University, Dept. of Astrophysics and Planetary Sciences, 800 E. Lancaster Ave, Villanova, PA 19085, USA*

<sup>3</sup>*Instituto de Astrofísica de Canarias, C. Vía Láctea, s/n, 38205 La Laguna, Santa Cruz de Tenerife, Spain*

(Received; Revised; Accepted)

Submitted to ApJS

### ABSTRACT

Spectroscopic observations constrain the fundamental properties of stellar atmospheres, in particular, the effective temperature, the gravitational acceleration, or the metallicity. In this work, we describe the spectroscopic module for Phoebe, which allows for modelling of spectra, either normalized, or in absolute units ( $\text{W m}^{-2} \text{m}^{-1}$ ). The module is based on extensive grids of synthetic spectra, taken from literature, which are interpolated and integrated over the surface. As an approximation, we assume that limb darkening is given by an analytical law, while other effects (e.g., eclipses) are treated self-consistently. Our approach is suitable for single stars, binaries, or multiples, and can be further extended to systems with pulsating components. **This draft refers to a development version of Phoebe, available at <https://github.com/miroslavbroz/phoebe2/tree/spectroscopy2>. It is not yet included in the official Phoebe repository!**

*Keywords:* stars: binaries: eclipsing – spectroscopy

### 1. INTRODUCTION

Models of eclipsing binaries are commonly constrained by two (or more) types of observations, e.g., by light curves and radial velocities, in order to obtain the absolute values of parameters (masses, radii, temperatures, orbit, or distance). A number of correlations among these parameters exist (Conroy et al. 2020), which could, in principle, significantly decrease the uncertainties of parameters (see, e.g., Suzuki et al. 2012). In particular, the gravitational acceleration at a stellar surface

$$g = \frac{Gm}{R^2} \quad (1)$$

is certainly correlated with the mass  $m$ , and the radius  $R$ ; the bolometric flux

$$\Phi = \left(\frac{R}{d}\right)^2 \sigma T_{\text{eff}}^4, \quad (2)$$

again, with the radius  $R$ , the distance  $d$ , and the effective temperature  $T_{\text{eff}}$ ; or more specifically, such relations also exist for individual passbands. Last but not least, chemical composition, internal structure, or pulsation frequencies, are closely related to the metallicity  $\mathcal{Z}$ . All these parameters could be constrained by spectroscopy.

A stellar atmosphere and its emergent spectrum is therefore parameterized by  $T_{\text{eff}}$ ,  $\log g$ ,  $\mathcal{Z}$ , and possibly also by the direction  $\mu \equiv \cos \theta$ , if a full field is available (Puls et al. 2005; Abdul-Masih et al. 2020; Abdul-Masih 2023). One can use existing tools for interpolation in grids of synthetic spectra, e.g., Pyterpol, previously used for  $\xi$  Tau (Nemravová et al. 2016; Brož 2017) and compare synthetic to observed spectra. However, it is still important to combine spectra with other datasets, otherwise the model would remain unconstrained, or poorly constrained.

In this work, we thus implement a spectroscopic module in Phoebe (Prša et al. 2016; Horvat et al. 2018; Jones et al. 2020; Conroy et al. 2020; Abdul-Masih et al. 2020) to improve modelling of binaries (or multiple systems). Apart from light curves and radial velocities, normalized (rectified) spectra and/or spectral-energy distributions (SED) could be used. Ideally, radial velocities should be entirely superseded by spectra, which encompass the same information.

## 2. METHODS

Single stars, binaries, or triples in Phoebe are all described by means of triangular meshes (Prša et al. 2016), which closely follow the Roche potential (Roche 1873; Kopal 1959; Horvat et al. 2018). Summing over triangles belonging to one component allows to compute also per-component properties. We thus have two options for the spectroscopic module, (i) complex, with integration of spectra over triangles; (ii) simplified, with just one spectrum per component. The former is much more precise, but the latter is fast.

### 2.1. Complex model

In our complex model, normalized synthetic spectra are generated for each triangle,

$$I_{\lambda,i} = \text{sg.get\_synthetic\_spectrum}(T_{\text{eff},i}, \log g_i, \mathcal{Z}_i) \quad \text{for } \forall i, \quad (3)$$

parametrized by  $T_{\text{eff}}$ , the local effective temperature,  $\log g$ , the local gravitational acceleration (in cgs units), and  $\mathcal{Z} = 10^{\text{abun}}$ , the component metallicity. Typically, more than 1000 spectra per component are needed. We note that the interpolation is not done in  $\mu$  and that the limb darkening is discussed elsewhere (see  $I_{\text{pass}}$  below).

The Doppler effect is accounted for in a standard way, as

$$\lambda' = \lambda \left( 1 + \frac{v_{\text{rad}}}{c} \right) \quad (4)$$

where  $v_{\text{rad}}$  is the radial velocity,  $c$  the speed of light. In our specific case, we apply neither instrumental broadening, since our synthetic spectra were broadened (to 0.01 Å), nor rotational broadening, since it is already accounted for in the radial motion of all triangles;  $I'_\lambda = I_\lambda$ .<sup>1</sup> Nevertheless, we always perform a piece-wise linear interpolation to the observed wavelengths ( $\lambda''$ )

$$I''_\lambda = \text{pyterpolmu.interpolate\_spectrum}(\lambda', I'_\lambda, \lambda''). \quad (5)$$

Finally, the normalized monochromatic flux is computed as

$$\Phi_\lambda = \frac{1}{L_{\text{tot}}} \sum_i I_{\text{pass},i} S_i \cos \theta_i f_i I''_{\lambda,i}, \quad (6)$$

where the sum is over triangles,  $I_{\text{pass},i}$  are the corresponding passband intensities, which are limb-darkened and gravity-darkened (i.e., the same as for light curve computations),  $S_i$  the surface areas,  $\cos \theta_i$  the cosines with respect to the local normals, and  $f_i$  fractions of triangles, which are visible.

*SED*—When computing SEDs, we must use a 2nd grid of *absolute* synthetic spectra, at stellar surface, in  $\text{erg s}^{-1} \text{cm}^{-2} \text{\AA}^{-1}$  units,

$$I_{\lambda,i} = \text{sg2.get\_synthetic\_spectrum}(T_{\text{eff},i}, \log g_i, \mathcal{Z}_i) \quad \text{for } \forall i. \quad (7)$$

The monochromatic flux, at Earth, in  $\text{W m}^{-2} \text{m}^{-1}$  units, is computed as

$$\Phi_\lambda = \frac{1}{\pi d^2} \sum_i \text{lds}_i S_i \cos \theta_i f_i I''_{\lambda,i}, \quad (8)$$

where  $d$  is the distance to the system,  $\text{lds}_i$  the limb darkening function values; the factor of  $\pi$  in the denominator is due to the surface area (cancelling with  $\pi R^2$ ), and an additional factor of  $10^7$  is due to units conversion.

Since we use our own synthetic spectra (i.e., not the atmospheres included in Phoebe) we have to account for the limb darkening by choosing an analytical limb-darkening law (linear, logarithmic, square-root, quadratic, or non-linear); the limb darkening coefficients should correspond to the range of  $\lambda$ , of course.

<sup>1</sup> Optionally, one may apply rotational broadening (Eq. (12)) to each triangle, according to its *differential* radial velocity of 3 vertices.

### 2.2. Simplified model

In our simplified model, we estimate component luminosities and use them as weights for component spectra. For simplicity, we compute the Planck function

$$B_\lambda = \frac{2hc^2}{\lambda^5} \frac{1}{\exp\left(\frac{hc}{\lambda k T_{\text{eff}}}\right) - 1} \quad (9)$$

and the monochromatic luminosity,

$$L_\lambda = \pi R^2 B_\lambda. \quad (10)$$

The respective synthetic spectrum, for  $\mu = 1$ , is obtained as

$$I_\lambda = \text{sg.get\_synthetic\_spectrum}(T_{\text{eff}}, \log g, \mathcal{Z}). \quad (11)$$

The Doppler effect is computed as before (Eq. (4)). We do not apply the instrumental broadening, but do apply the rotational broadening,

$$I'_\lambda = 1 - \mathcal{F}^{-1}[\mathcal{F}(1 - I_\lambda) \mathcal{F}(K)], \quad (12)$$

where the fast Fourier transform is used (instead of convolution). The respective kernel (Díaz et al. 2011)

$$K = \frac{2}{\pi} \frac{(1 - \epsilon)\sqrt{\arg} + \frac{\pi}{2}\epsilon \arg}{v_{\text{rot}}/c(1 - \frac{1}{3}\epsilon)}, \quad (13)$$

where  $v_{\text{rot}} \equiv \Omega R \sin i_\star$  is the projected rotation velocity,  $\arg \equiv 1 - (v/v_{\text{rot}})^2$ ,  $\epsilon$  the linear limb-darkening coefficient; the wavelength scale is equidistant in  $\log \lambda$ . The kernel normalisation is done *ex-post*. The interpolation to the observed wavelengths is as before (Eq. (5)).

Finally, the normalized monochromatic flux is computed as

$$\Phi_\lambda = \frac{1}{L_{\text{tot}}} \sum_i L_{\lambda,i} I''_{\lambda,i}, \quad (14)$$

where the sum is over components.

*SED*—Likewise, we obtain absolute synthetic spectra, at stellar surface, as in Eq. (7). The monochromatic flux, at Earth, is then

$$\Phi_\lambda = \frac{1}{d^2} \sum_i R_i^2 I''_{\lambda,i}. \quad (15)$$

The monochromatic flux can be compared to spectroscopic observation, or to narrow-passband photometry, provided it is converted to the same units (i.e., calibrated, divided by  $\Delta\lambda$ ), the object does have too strong spectral features (within  $\Delta\lambda$ ), and interstellar extinction is properly taken into account (Jones et al. 2020).

### 2.3. Implementation notes

We introduced two new datasets in Phoebe, SPE and SED. The corresponding quantities `wavelengths`, `fluxes` were exposed to users (as ‘twigs’). For example, `fluxes = b['fluxes@spe01@phoebe01@latest@spe@model'].value`, or alternatively, `fluxes = b.get_value('fluxes', dataset='spe01', context='model')`. Further examples are available as Jupyter notebooks.

Among the grids, which can be used in Phoebe, are OSTAR (Lanz & Hubený 2003), BSTAR (Lanz & Hubený 2007), AMBRE (de Laverny et al. 2012), POLLUX (Palacios et al. 2010), PHOENIX (Husser et al. 2013), or POWR (Hainich et al. 2019). They can be downloaded from <http://sirrah.troja.mff.cuni.cz/~mira/xitau/> as text files, which are automatically converted to binary (npz), so that next time they are read fast. In order to use them in Phoebe, one must prepare a user-defined `gridlist`, which is a list of files and their associated parameters ( $T_{\text{eff}}$ ,  $\log g$ ,  $\mathcal{Z}$ , or  $\mu$ ).

The sampling of the normalized and absolute grids is 0.01 Å and 0.1 Å, respectively. Both grids were prepared with the instrumental broadening of this level. Only the former is suitable for fitting of narrow spectral lines, while the latter is sufficient in wide spectral lines (like Balmer) and continuum. It is important that the observed resolution is similar ( $\sim 0.01$  Å), otherwise narrow spectral lines attributed to individual triangles would be poorly sampled, which

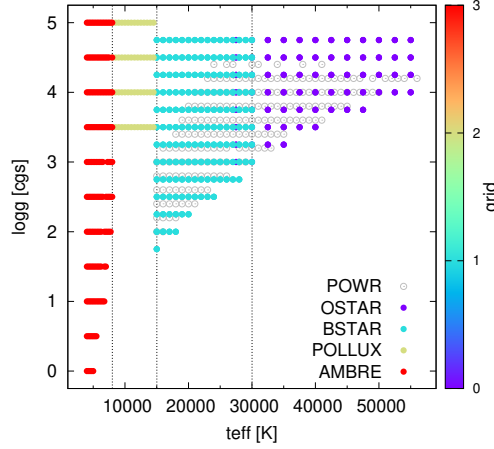


**Figure 1.** Coverage of the existing grids of normalized synthetic spectra, in terms of the effective temperature  $T_{\text{eff}}$  vs. the gravitational acceleration  $\log g$ . The metallicity  $\mathcal{Z}$  is solar.

creates spurious numerical noise, or ‘wavy’ artifacts. On the other hand, if the observed resolution is low, one may optionally apply additional instrumental or rotational broadening of synthetic spectra during fitting, which, however, makes it somewhat slower (see also Fig. 8).

The coverage of the normalized grids is demonstrated in Fig. 1. There are a few regions, where the grids overlap and one can expect some “jumps”, which might be negatively affecting a convergence. This occurs around 30000 K, where OSTAR and BSTAR grids overlap, and also around 15000 and 8000 K. If this problem occurs, one could comment lines in the `gridlist` to prefer one or the other grid.

Internally, we use `Ndpolator`<sup>2</sup> for linear interpolation or extrapolation in an  $n$ -dimensional space. It is as fast as possible (implemented in C), allowing for a presence of “voids” (i.e., a non-uniform grid). For safety, the extrapolation method is set to the nearest-neighbor.

### 3. EXAMPLES

#### 3.1. Comparison of complex vs. simplified models

The first example is a normalized synthetic spectrum  $\Phi_\lambda$  obtained for the default binary in Phoebe (Fig. 2). At the phase 0.25, the respective spectral lines are double, but since it is a relatively cool atmosphere (6000 K) the numerous metallic lines (Fe, Ti, Th, ...) overlap and are thus heavily blended. Both our models, complex and simplified, agree very well, because the components are spherical, the effective temperatures and  $\log g$  values are constant, which implies that all spectra are the same, only Doppler-shifted and integrated over the surface (i.e., equivalent to the rotational broadening).

In the case of absolute synthetic spectra  $\Phi_\lambda$  (in  $\text{W m}^{-2} \text{m}^{-1}$  units), the comparison is different (Fig. 3). The simplified model is slightly offset with respect to the complex model, due to slight differences in absolute luminosities (passband vs. planckian). However, our models differ at the phase zero, when the two components are totally eclipsed; in this case, the simplified model is incorrect (by a factor of 2).

#### 3.2. Flux calibration

The second example is a flux calibration computed for the Sun at 1 au distance (Fig. 4). Its synthetic spectrum was interpolated from the PHOENIX grid; it agrees well with other solar spectra (Gueymard 2003). Its integral over wavelengths,  $\Phi = \int \Phi_\lambda d\lambda \doteq 1338 \text{ W m}^{-2}$ , is close to the measured solar constant,  $(1360.8 \pm 0.5) \text{ W m}^{-2}$  (Kopp & Lean 2011).

#### 3.3. Limb darkening

Limb darkening primarily affects SEDs, as shown in Fig. 5, where the decrease of the absolute flux  $\Phi_\lambda$  is proportional to the limb darkening coefficient  $\epsilon$ , as expected. Even though this approach is not self-consistent, because the respective

<sup>2</sup> <https://github.com/aprsa/ndpolator>

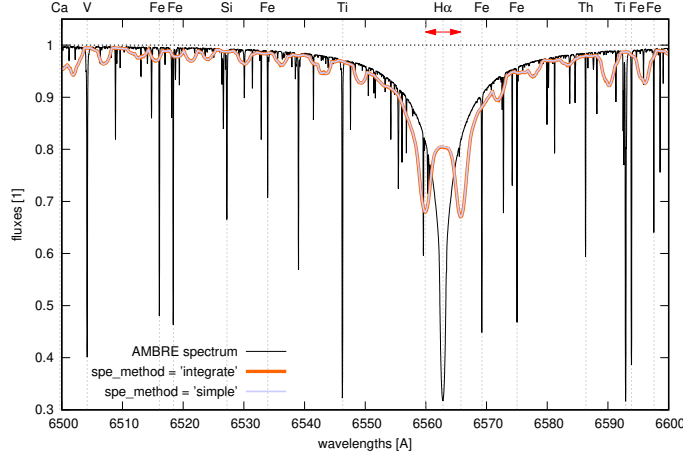


**Figure 2.** Basic example of the normalized flux  $\Phi_\lambda$  over the wavelength  $\lambda$  (in angströms), computed for the default binary in Phoebe (i.e.,  $P = 1$  d,  $a = 5.3 R_\odot$ ,  $m_1 = m_2 \doteq 0.998813 M_\odot$ ,  $R_1 = R_2 = 1 R_\odot$ ,  $T_1 = T_2 = 6000$  K,  $\log g_1 = \log g_2 \doteq 4.437$ ). At the phase 0.25, the lines of components are shifted by the radial velocity amplitudes,  $K_1 = K_2 \doteq 134 \text{ km s}^{-1}$ , as indicated by the red arrow. The original, unrotated synthetic spectrum from the AMBRE grid (de Laverny et al. 2012) is also plotted (black). Line identifications were taken from [https://bass2000.obspm.fr/solar\\_spect.php](https://bass2000.obspm.fr/solar_spect.php).

atmospheres also imply the limb darkening (for  $\mu \rightarrow 0$ ), the full field is not always available. Moreover, it would require much more extensive, 4-dimensional grids (for all  $\mu$ 's). For reference, the current grids represent 10 and 14 GB of uncompressed data, respectively (for  $\mu = 1$ ). We thus consider our approach to be a good compromise.

### 3.4. Rotation

Rotation affects both SEDs and normalized spectra (see Fig. 6). Neither the effective temperature  $T_{\text{eff}}$ , nor the gravitational acceleration  $\log g$  are constant on the surface (von Zeipel 1924), and spectra must be varied accordingly. The poles are hotter than the equator, which leads to observable effects especially in UV, e.g., for Vega (Aufdenberg et al. 2006). In particular, the limb darkening of poles (for  $i_* \rightarrow 0$ ) must be accounted for, as it constrains the inclination of the spin axis. On top of this, rotation induces Doppler shifts of triangles, resulting in a rotation broadening of lines, as expected.

### 3.5. Eclipses

Finally, we computed normalized synthetic spectra in the course of an eclipse (Fig. 7). The simplified model is again incorrect; only the complex model shows asymmetries of line profiles due to the partially eclipsed surfaces. For the default binary, this applies to the phases  $\phi \in (0; 0.06)$ . One can expect even more pronounced asymmetries if the respective binary is contact (Abdul-Masih et al. 2020), if one of the components is fast-rotating, or whenever the temperature difference is substantial.

## 4. CONCLUSIONS

We have described the spectroscopic module of Phoebe, along with a few examples, how to use it. Using more datasets (LC, RV, SPE, SED) at the same time means that models of binaries shall be better constrained, because spectra and spectral lines contain detailed information about stellar atmospheres; more detailed than light curves and radial velocities.

On the other hand, one should be honest about it, more datasets sometimes means more problems — if systematic errors are present. Spectroscopy is not a fully independent measurement, precisely orthogonal to other types of data. For example, radial velocities suffer from systematics when lines are blended; or spectra themselves might be uncertain, due to their calibration, normalisation, or rectification (see, e.g., Worley et al. 2012; Sacco et al. 2014; Jönsson et al. 2020).

This version of Phoebe also opens the possibility to fit pulsations spectroscopically, if the radial velocities at the surface are perturbed, creating waves travelling across line profiles (Maintz et al. 2003; Aerts et al. 2010). This fitting might be problematic though, if the underlying model for pulsations is insufficient, e.g., for fast-rotating stars (Aerts & Tkachenko 2023).

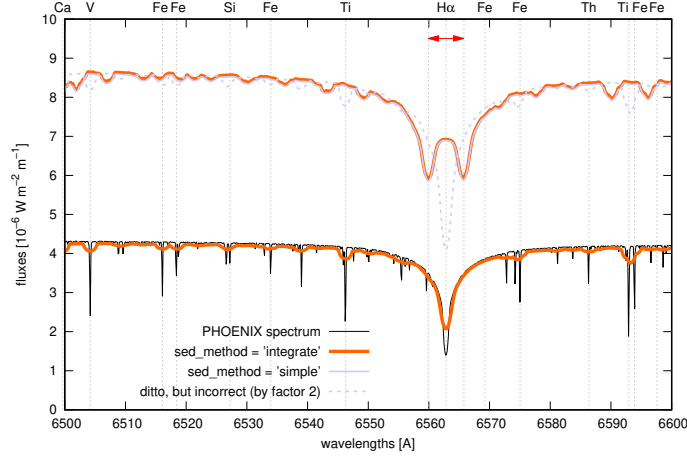


**Figure 3.** Same as Fig. 2, but for the absolute flux  $\Phi_\lambda$  (in  $\text{W m}^{-2} \text{m}^{-1}$ ) over the wavelength  $\lambda$ . Phases 0 (total eclipse) and 0.25 (out of eclipses) are shown for comparison. The complex model (orange) correctly computes a factor of 2 difference in  $\Phi_\lambda$ , but the simplified model (gray, dashed) is unable to account for any eclipses. The original, unrotated synthetic spectrum from the PHOENIX grid (Husser et al. 2013) is also plotted (black).

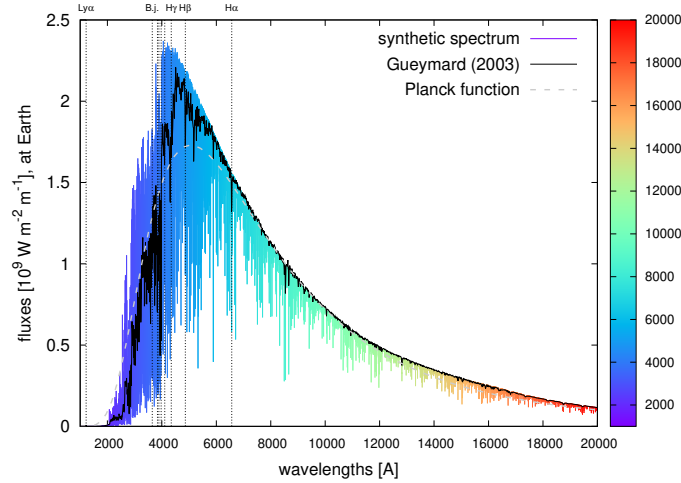


**Figure 4.** Flux calibration example computed for the Sun at 1 au distance. The peak monochromatic flux  $\Phi_\lambda \doteq 2 \times 10^{-9} \text{ W m}^{-2} \text{m}^{-1}$  is correct. For comparison, we plot the synthetic solar spectrum from Gueymard (2003) (black) and the Planck function (gray) for the effective temperature  $T_{\text{eff}} = 5770 \text{ K}$ .

This work has been supported by the Czech Science Foundation through grant 25-16507S (M. Brož).

## REFERENCES

- Abdul-Masih, M. 2023, *A&A*, 669, L11
- Abdul-Masih, M., Sana, H., Conroy, K. E., Sundqvist, J., Prša, A., Kochoska, A., & Puls, J. 2020, *A&A*, 636, A59
- Aerts, C., Christensen-Dalsgaard, J., & Kurtz, D. W. 2010, *Asteroseismology* (Springer Science+Business Media B.V.)
- Aerts, C., & Tkachenko, A. 2023, *arXiv e-prints*, arXiv:2311.08453
- Aufdenberg, J. P., et al. 2006, *ApJ*, 645, 664
- Brož, M. 2017, *ApJS*, 230, 19
- Conroy, K. E., et al. 2020, *ApJS*, 250, 34
- de Laverny, P., Recio-Blanco, A., Worley, C. C., & Plez, B. 2012, *A&A*, 544, A126
- Díaz, C. G., González, J. F., Levato, H., & Grosso, M. 2011, *A&A*, 531, A143
- Gueymard, C. A. 2003, *Solar Energy*, 74, 355

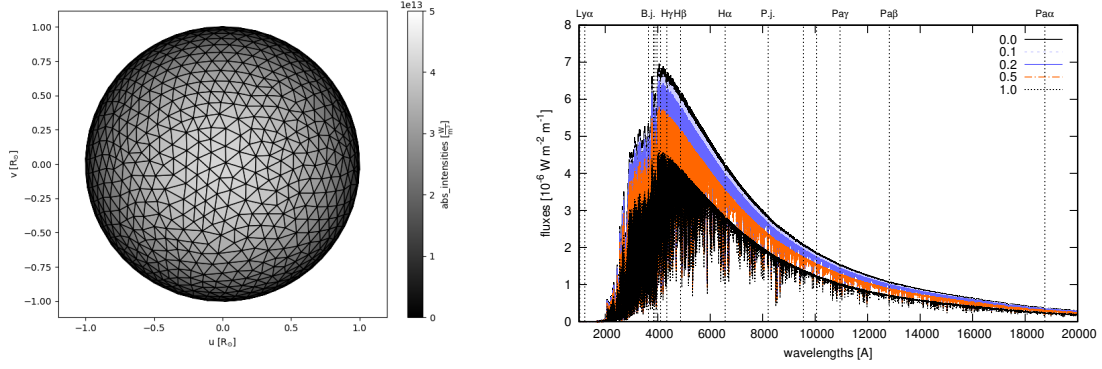


**Figure 5.** Limb-darkening example computed for the default star in Phoebe (i.e.,  $m = 1 M_{\odot}$ ,  $R = 1 R_{\odot}$ ); observed at a distance of 100 pc. Limb darkening coefficients were set to manual, linear; the values 0.0, 0.1, 0.2, 0.5, 1.0 were tested. The SED changes as expected.

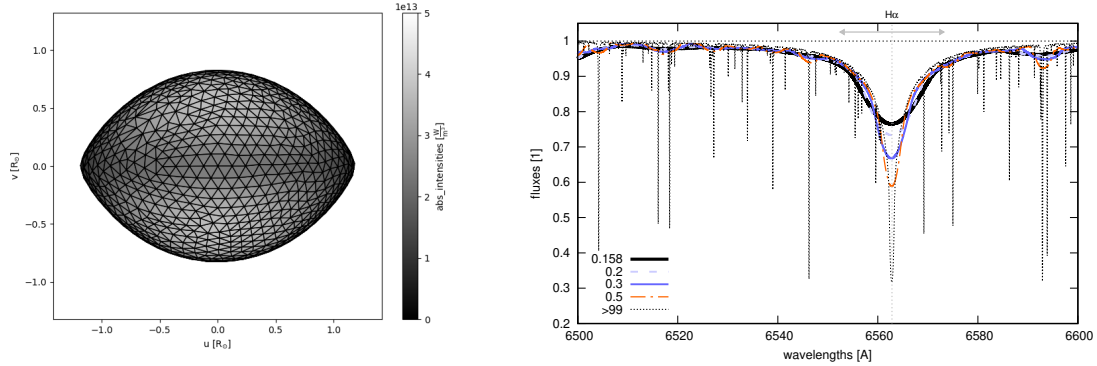


**Figure 6.** Rotation example computed for the default star in Phoebe. The rotation period values 0.16 (close to critical), 0.20, 0.30, 0.50, and  $>99$  days were tested. The spectral lines change as expected.

Hainich, R., Ramachandran, V., Shenar, T., Sander, A. A. C., Todt, H., Gruner, D., Oskinova, L. M., & Hamann, W. R. 2019, *A&A*, 621, A85  
 Horvat, M., Conroy, K. E., Pablo, H., Hambleton, K. M., Kochoska, A., Giammarco, J., & Prša, A. 2018, *ApJS*, 237, 26  
 Husser, T. O., Wende-von Berg, S., Dreizler, S., Homeier, D., Reiners, A., Barman, T., & Hauschildt, P. H. 2013, *A&A*, 553, A6  
 Jones, D., et al. 2020, *ApJS*, 247, 63  
 Jönsson, H., et al. 2020, *AJ*, 160, 120  
 Kopal, Z. 1959, *Close binary systems* (The International Astrophysics Series, London: Chapman & Hall)  
 Kopp, G., & Lean, J. L. 2011, *Geophys. Res. Lett.*, 38, L01706  
 Lanz, T., & Hubený, I. 2003, *ApJS*, 146, 417  
 —. 2007, *ApJS*, 169, 83

Maintz, M., Rivinius, T., Štefl, S., Baade, D., Wolf, B., & Townsend, R. H. D. 2003, *A&A*, 411, 181  
 Nemravová, J. A., et al. 2016, *A&A*, 594, A55  
 Palacios, A., Gebran, M., Josselin, E., Martins, F., Plez, B., Belmas, M., & Lèbre, A. 2010, *A&A*, 516, A13  
 Prša, A., et al. 2016, *ApJS*, 227, 29  
 Puls, J., Urbaneja, M. A., Venero, R., Repolust, T., Springmann, U., Jokuthy, A., & Mokiem, M. R. 2005, *A&A*, 435, 669  
 Roche, É. 1873, *d'Essai sur la constitution et l'origine du système solaire* (Montpellier: Boehm et fils)  
 Sacco, G. G., et al. 2014, *A&A*, 565, A113  
 Suzuki, N., et al. 2012, *ApJ*, 746, 85  
 von Zeipel, H. 1924, *MNRAS*, 84, 665  
 Worley, C. C., de Laverny, P., Recio-Blanco, A., Hill, V., Bijaoui, A., & Ordenovic, C. 2012, *A&A*, 542, A48



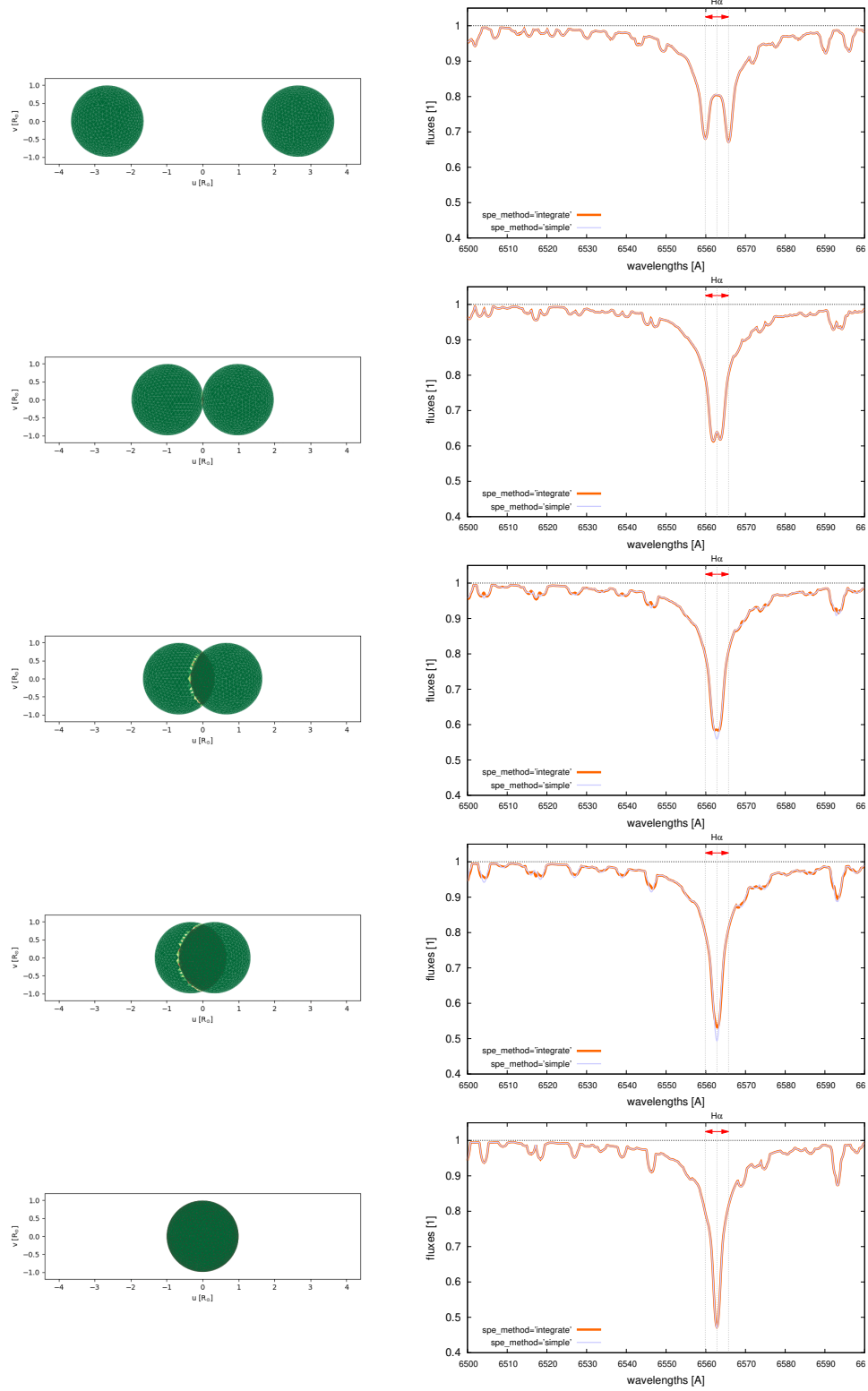


**Figure 7.** Eclipse example computed for the default binary in Phoebe. Left: Meshes with the fractions of triangles, which are visible. Right: Normalized synthetic normalized spectra  $\Phi_{\lambda}$  (orange) over the wavelength  $\lambda$ . During the eclipse, line profiles of the components are blended. While a simplified model (gray) is just a sum of profiles, the complex model correctly computes asymmetries arising due to eclipsed parts of the surface.



## APPENDIX

## A. SUPPLEMENTARY FIGURES

In Fig. 8, we show how sampling of  $\lambda$  and mesh resolution affect resulting synthetic spectra integrated over triangles.

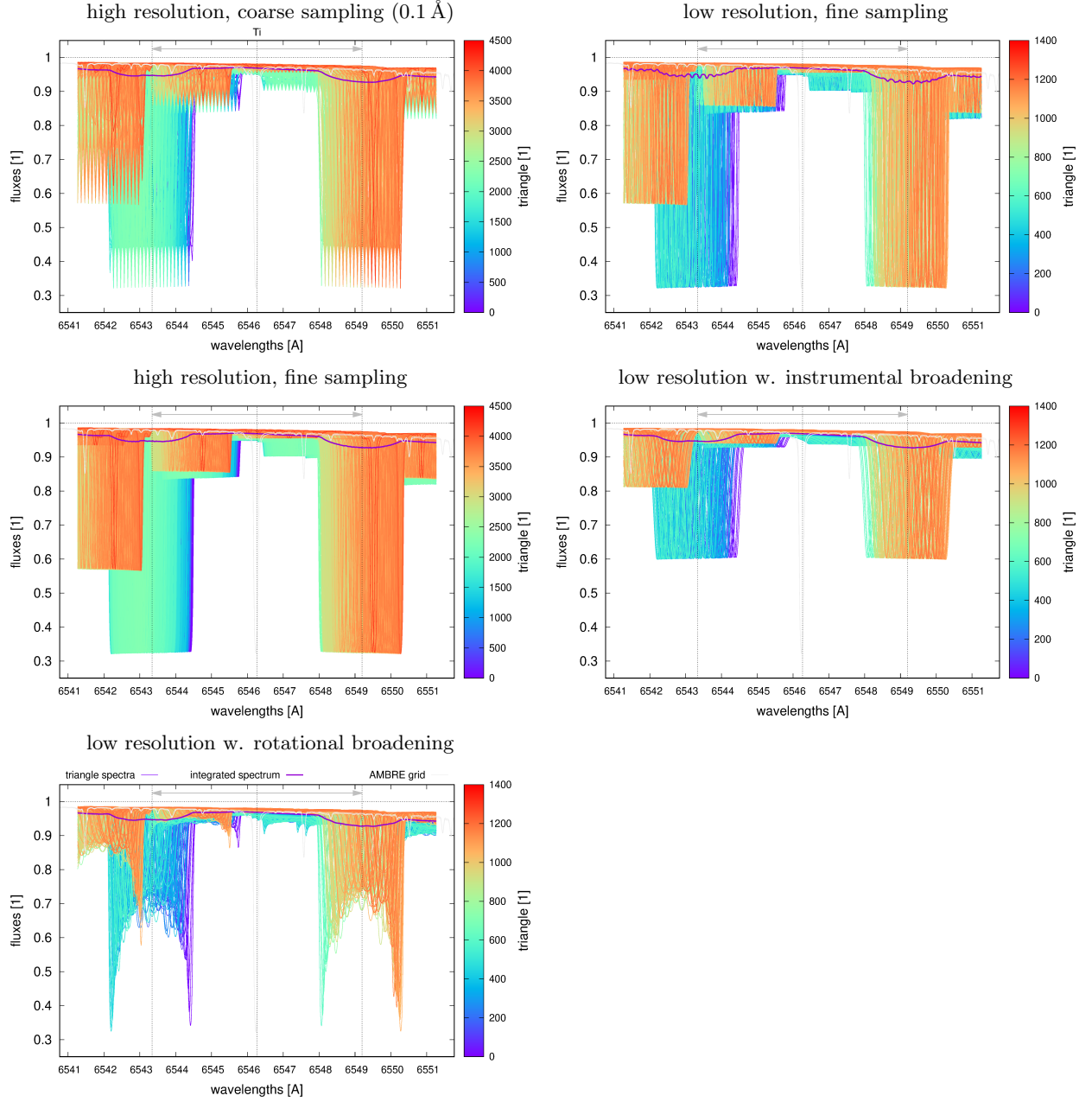


**Figure 8.** Synthetic spectra for non-optimal sampling of  $\lambda$  or mesh resolution. Top left: If the resolution is high (2000 triangles per component), but the sampling is too coarse (0.1 Å), spectra of individual triangles with narrow lines are poorly sampled, but the resulting integrated spectrum seems acceptable. Top right: If the resolution is too low (500 triangles), even with fine sampling (0.01 Å) doppler-shifted triangles do not sum up smoothly and ‘wave-like’ artifacts occur. Middle left: One can solve it by using both high resolution and fine sampling. Middle right: Or, by using low resolution with instrumental broadening (fwhm = 0.2 Å). Bottom left: Or, by using low resolution with rotational broadening, according to a differential radial velocity of each triangle (3 vertices), which makes spectral lines of individual triangles wide enough, so that the resulting integrated spectrum seems again acceptable.